

## Electron kinetics in simple liquids at high electric fields

E. E. Kunhardt

*Weber Research Institute, Polytechnic University, Farmingdale, New York 11735*

(Received 9 January 1991; revised manuscript received 30 April 1991)

A model for the motion of an electron in a simple liquid is presented. It is used in the Monte Carlo simulation of the behavior of an assembly of electrons in liquid argon subjected to high electric fields. To implement this simulation, a set of scattering rates for electrons have been obtained. Electron-energy distribution, transport parameters (drift velocity, longitudinal, and transverse diffusion coefficients), and ionization rate have been calculated. The distribution function has been found to be far from the usually assumed Maxwellian form. For fields above 10 kV/cm, the drift velocity decreases with increasing field, changing to a positive slope for fields above approximately 500 kV/cm. At higher fields, the ratio of the longitudinal to transverse diffusion coefficient becomes greater than 1. These observations are a consequence of having, with increasing field, a maximum in the backscattering rate, and an increasing number of electrons with energies above that corresponding to the maximum in the total scattering rate. The threshold field for ionization has been calculated to be approximately 2 MV/cm.

### I. INTRODUCTION

Understanding the behavior of an assembly of excess electrons immersed in a liquid background and under the influence of an external electric field is of fundamental importance for liquid-state electronics. To formulate a statistical description of the behavior of the assembly, it is necessary to obtain a description for the state of an electron belonging to the assembly and for its evolution under the action of the field. Two physical approaches have evolved for addressing these issues in simple liquids; namely, as perturbations of similar problems in crystalline solids and dilute gases.<sup>1-7</sup> In the gas picture, the liquid is viewed as a dense gas (the perturbation parameter being the ratio of the electron wavelength to the scattering free path),<sup>1-4</sup> whereas in the solid picture the liquid is viewed as a crystal with static (zero-energy) density fluctuations (the perturbation parameter being the magnitude of the density fluctuation).<sup>5-7</sup>

A number of macroscopic models have been proposed to extend the above approaches to more complex situations.<sup>8-14</sup> These models are based primarily on either percolation theory<sup>8,9</sup> or on the assumption that a state of dynamic equilibrium exists among the available electron states.<sup>10-14</sup> Even in situations where the perturbation approaches are satisfactory, the complex nature of the electron-liquid interactions must be greatly simplified in order to arrive at tractable descriptions. These simplifications are most severe in molecular liquids since the interactions are sensitive to the shape and the polar nature of the molecule.

The descriptions that have been developed have been used mainly to investigate the behavior of the drift velocity of the assembly as a function of electric field, temperature, density (pressure), and, in a limited sense, the nature of the liquid. This focus derives from the fact that the experimental investigations have concentrated on measurements of the drift velocity<sup>15-19</sup> and transverse diffusion

coefficient<sup>20</sup> under a variety of conditions. The drift velocity of the assembly of electrons in liquids has been observed to vary over 7 orders of magnitude.<sup>21</sup> This range results, qualitatively, from the ionlike behavior of the electrons in strongly polar liquids (such as water) to the Bloch-state-like behavior in some liquid rare gases (argon, for example). Although in some cases qualitative agreement has been obtained, considerable work remains in the development of theoretical models that explains the wide range of behavior that has been observed. These results have been reviewed in a number of articles.<sup>21-23</sup>

In this paper a model for the motion of an electron in a simple liquid is presented and used in the Monte Carlo simulation of the behavior of an electron assembly in liquid argon at high electric fields. To implement this simulation, a set of scattering rates for electrons have been obtained. These topics are discussed in Secs. II-IV. Results for the energy distribution of electrons, transport parameters (drift velocity and transport coefficients), and average ionization rate are presented in Sec. V, followed by concluding remarks.

### II. SEMICLASSICAL MODEL FOR ELECTRONS IN SIMPLE LIQUIDS

A useful approach for describing the behavior of an assembly of noninteracting electrons in a background medium is to first determine the allowed stationary states for a single electron, and then represent, in terms of these states, the evolution of the electron under the influence of what are then considered to be potential perturbations. These two problems are closely related since they result from the standard separation of the Hamiltonian describing the system into two parts, one of which is treated as a perturbation.<sup>24</sup>

Consider the continuum energy states corresponding to ionization of an isolated atom, i.e., infinite interatomic separation (see Fig. 1). These states are characterized by

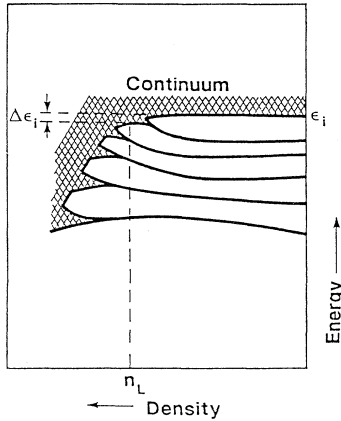


FIG. 1. Schematic representation of the behavior of representative isolated-atom electron states vs density. Their behavior with density is indicated by the solid lines. At liquid densities only one conduction band is assumed.

plane-wave functions (i.e., free-electron wave functions), and may formally be considered to form a band (the “conduction band” in the Bloch scheme<sup>25</sup>) with no energy upper limit and lower limit given by the ionization potential  $\epsilon_i$ . These (stationary) states are identified by the conjugate coordinates  $(\mathbf{r}, \mathbf{p})$ , where  $\mathbf{r}$  is position and  $\mathbf{p}$  is the momentum ( $\mathbf{p} = \hbar \mathbf{k}$ , where  $\hbar$  is Planck’s constant divided by  $2\pi$  and  $\mathbf{k}$  is the wave number of the associated plane-wave function). The energy-momentum relation,  $\epsilon = \epsilon(\mathbf{p}) = \epsilon(\mathbf{k})$ , for these states is parabolic and isotropic. That is,

$$\epsilon = \frac{p^2}{2m} = \frac{\hbar^2 k^2}{2m}, \quad (1)$$

where  $m$  is the electronic mass. The relation between acceleration and the applied field is given by Newton’s law

$$\frac{d\mathbf{p}}{dt} = \frac{d(\hbar \mathbf{k})}{dt} = -e \mathbf{E}, \quad (2)$$

where  $-e$  is the charge of the electron and  $\mathbf{E}$  is the applied electric field.

In dilute gases, such that the interparticle separation is still large, but finite, the stationary electron states can be taken to be the same as those for the isolated atom (free-electron states), and the density of these states (per unit energy interval) is also taken to be a continuous function of energy going to zero at the band edge. The gas atoms (and the applied field) are treated as isolated potential perturbations that cause transitions between these states. In addition, these atoms may introduce localized states at their location leading to negative ion formation. (It is also possible, in principle, to have localized states at the bottom of the “conduction” band due to multiple scattering<sup>26</sup> as discussed below for the condensed phase.)

In those crystalline solids for which the Bloch scheme is useful, the description of electron behavior is formally the same as for dilute gases.<sup>25,27</sup> In the case of solids, the free-electron band extends to lower energies than in the gas phase (to the bottom of the usual conduction band)

and gaps appear in the energy-momentum relation, Eq. (1) (this relation may no longer be parabolic nor isotropic for all energies). This results from the inclusion of part of the microscopic scattering potential in the definition of the stationary free-electron states.<sup>25,27</sup> Thus, the perturbing potentials causing transitions between the states have a different origin than in the dilute gas (where the complete scattering potential is treated as a local perturbation). Consequently, for both medium (when the resulting scattering rates are, by design, not large), the statistical description of the behavior of the electron assembly can be effected within the framework of kinetic theory, and in particular, the Boltzmann equation.<sup>25,27</sup> In the presence of localization (i.e., negative ion formation in the gas and trapping in the solid) and when the dynamics of the localized states can be treated within a similar framework, this approach can also be used by grouping the electrons into subassemblies according to the nature of the states.

The description of electron behavior in simple liquids follows from the above discussion. To formulate this description, the energy-momentum relation for the free-electron states (and possible localized states), and the perturbing potentials causing transitions between them, need to be determined. Of particular interest is the question of whether or not the energy-momentum relation contains energy gaps (as in solids) since it has a significant effect on the threshold for impact ionization in the liquid phase. To qualitatively answer some of these issues, consider what happens to the free-electron (conduction) band and discrete (bound-electron) states of a system of atoms as the interatomic separation is reduced from infinity to that which exists in a simple fluid.<sup>27,28</sup> The free-electron band broadens downward toward low energies (see Fig. 1), overlapping the high-energy discrete (Rydberg) states which are themselves broadening. Consequently, the bottom of the band is lower than in the dilute gas phase. The question arises as to whether or not any of the lower-lying discrete energy states, which are not overlapped by the free-electron band, is sufficiently broadened to be considered a band of free-electron states. Measurements of the low energy limit of the free-electron band in simple liquids show that it changes by a few tenths of an eV in going from a dilute gas to a liquid.<sup>29</sup> It is then reasonable to assume that the lower-lying (in energy) discrete levels remain degenerate, albeit shifted in energy from their values in the dilute gas phase. This is schematically shown in Fig. 1, where  $n_L$  corresponds to the density of the liquid. The disordered structure of the medium becomes more pronounced than in the gas phase in that the density of states at the bottom of the band has a tail similar to that found in amorphous semiconductors,<sup>30</sup> and which indicates the presence of localized electron states (such tail should also exist in dilute gases, although at extremely low energies<sup>26</sup>).

Thus, as for gases and crystalline solids, the description of the behavior of an electron assembly in a liquid in general requires the use of coupled subassemblies for free and localized (trapped or attached) electrons. These subassemblies are represented by time dependent, semiclassical distribution functions  $f_f(\mathbf{r}, \mathbf{p}, t)$  and  $f_l(\mathbf{r}, \epsilon_l, t)$  for

free and localized electrons, respectively, where  $\varepsilon_l$  corresponds to the energy level of the  $l$ th localized state. In this paper the contribution from trapped electrons is not taken into account. In simple liquids,  $\varepsilon_l$  is below the meV range, so that for the fields of interest in this paper (with free-electron energies in the eV range), their contribution is expected to be small. This is presently being investigated.

Given the initial distribution of electrons over the free-electron states, the distribution at any other time may be obtained from either Monte Carlo simulation,<sup>31–33</sup> or from solution of the Boltzmann transport equation (BTE)<sup>25,27,34</sup> by either iterative or analytical techniques. At present, the Monte Carlo approach has a number of advantages over the BTE approach: It is relatively easy to implement at six-dimension ( $\mathbf{r}, \mathbf{p}$ ) space simulation, it can be easily modified to accommodate any number of interactions between the electrons and the background, and it provides considerable physical insight into the behavior of the electrons, including fluctuation phenomena.

To implement either approach, the energy-momentum relation for the free-electron states (the “conduction band,” in the sense discussed earlier) and the effect of perturbing potentials on these states (the scattering rates) need to be determined. These two issues are of course related. The model to be used for the energy-momentum relation has the following properties: (1) is more characteristic of the band in a dilute gas for the higher energy electron states (i.e., parabolic, isotropic, and with effective mass equal to the electronic mass), (2) takes into account multiple scattering toward the bottom of the band via an effective mass and thus becomes more characteristic of the condensed phase (with effective mass different from the electronic mass), and (3) has no energy gaps. The transition region (in energy) between the two types of behavior may be approximately delineated from scattering considerations (since this determines how the Hamiltonian is partitioned for defining the free-electron states and the scattering potentials). For electron energies such that the electron wave packet extends over a distance that is less than one or two times the interatomic separation, the free-electron states are taken to be those of the dilute gas and the microscopic (atomic) potentials are treated as perturbations causing transitions between these states. In this energy range, the transition probability between states  $\mathbf{k}$ , and  $\mathbf{k}'$ ,  $W_{\mathbf{k},\mathbf{k}'}$ , is obtained using Van Hove’s formulation.<sup>35,36</sup> In the low-energy range, multiple-scattering effects become important and it is then useful to incorporate part of this scattering into the energy-momentum relation by treating the liquid as a disordered crystal, as done by Basak and Cohen.<sup>5</sup> The transition probability in this range is then obtained by using deformation-potential theory.<sup>5,6</sup>

### III. THE MONTE CARLO TECHNIQUES

#### A. Tracking the electrons

In the kinetic description of the behavior of the electron assembly, the objective is to determine the distribu-

tion function at time  $t$ , knowing its form at an earlier time,  $t_0$ . In the Monte Carlo approach, a number of test electrons are selected to represent the initial distribution (typically 2000–3000), and their evolution simulated using statistical methods.<sup>32</sup> The trajectory of a free electron in the time interval from  $t_0$  to  $t$  is viewed as consisting of a series of “free flights,” each terminated by a scattering event. It is assumed that this flight, however small, exists. (In the limit of very large scattering rates, where the flights become infinitesimal, the free-electron states would have to be redefined.)

The equation of motion during the free flights is Eq. (1), with the electron velocity,  $\mathbf{v}$ , given by

$$\mathbf{v} = \nabla_{\mathbf{p}} \varepsilon(\mathbf{p}). \quad (3)$$

As discussed in the previous section, the model chosen for the energy-momentum relation of a free electron is as follows:

$$\varepsilon(1 + \alpha\varepsilon) = \frac{\hbar^2 k^2}{2m^*}, \quad \varepsilon < \varepsilon_t; \quad (4a)$$

$$\varepsilon = \beta k + \frac{\hbar^2}{2m} (k - k_0)^2, \quad \varepsilon > \varepsilon_t; \quad (4b)$$

where  $\alpha$  is the nonparabolicity parameter,  $m^*$  is the effective mass of the electrons at the bottom of the band,  $\varepsilon_t$  is the energy above which multiple scattering is not incorporated into the effective mass,  $k_t$  is the value of  $k$  at  $\varepsilon = \varepsilon_t$  from Eq. (4a), and  $\beta$  is chosen to assure continuity at  $\varepsilon = \varepsilon_t$ . To obtain continuity in velocity,  $\alpha$  is taken to be larger than  $1/\varepsilon_t$ , in which case  $\beta \sim \hbar\sqrt{2\alpha m^*}$ . The values chosen for these parameters are discussed in Sec. IV. Equation (4) represents a nonparabolic energy band with spherical constant surfaces. It reduces to parabolic relations at both high and low energies with effective masses equal to the electronic mass (characteristic of the gas phase) and  $m^* \sim 0.75m$  (Ref. 37) (characteristic of the condensed phase at a density of  $2.12 \times 10^{22} \text{ cm}^{-3}$ ), respectively. Equation (4a) is often used as a model for the energy-momentum relation in semiconductors.<sup>33</sup>

The potentials not included in the definition of the dispersion relation (i.e., free-electron states) cause deviations from the free-flight trajectory defined by Eq. (1), i.e., they give rise to the scattering events that terminate each free flight. The duration of a free flight,  $t_s$ , is determined from the probability for the occurrence of such an event via the relation<sup>32</sup>

$$R_1 = 1 - \exp \left[ - \int_0^{t_s} \Gamma_T[\varepsilon(t)] dt \right], \quad (5)$$

where  $R_1$  is a uniformly distributed random number in the interval  $[0,1]$  and  $\Gamma_T$  is the total scattering rate, which is a function of the time-dependent electron energy. Since the integral in Eq. (5) cannot in general be evaluated analytically, an explicit expression for  $t_s$  cannot be obtained. An alternate approach is to reformulate Eq. (5) in terms of the momentum change due to the action of the applied field during the time  $t_s$ . A modified self-scattering approach can then be used to explicitly evaluate this change. Details of this approach are given in

Ref. 33. A scattering event in general causes a discontinuous change in the energy and momentum of the electron. The outcome of the event specifies the initial conditions for the subsequent free flight. This outcome is determined from the probability distribution for the type of event and the differential scattering rates for each event. These rates and probability distribution are given in Sec. IV.

### B. Sampling of information

For the purpose of extracting information, the simulation is divided into time sections of length  $t_i$ . Since the position and momentum of each electron are known (at any time), the representative assembly is completely characterized. To compute the energy distribution of the assembly, the particles are sampled four times during a time section. An averaged distribution over the section is thus obtained, whose "coarseness" is determined by  $t_i$  ( $t_i$  is chosen between  $10^{-13}$  and  $10^{-12}$  sec, depending on the scattering rate in the energy range of interest for a given applied field). This "averaged" distribution is used in the calculation of the macroscopic ionization rate.

The mean energy of the electrons is computed by sampling the assembly once at the end of the section, i.e., at  $t_i$ . The center of mass of the electron assembly  $Z_c$ , the averaged squared radial deviation from the axis  $\langle R^2 \rangle$ , and the averaged squared longitudinal deviation from the center of mass  $\langle (Z - Z_c)^2 \rangle$ , are also calculated at the end of the time section. The values for the drift velocity  $W$ , the transverse diffusion coefficient  $D_T$ , and the longitudinal diffusion coefficient  $D_L$ , are obtained, in steady state, from the slopes of the least-squares straight-line fit to the  $Z_c$ ,  $\langle R^2 \rangle$ , and  $\langle (Z - Z_c)^2 \rangle$  versus time data, respectively;<sup>32</sup> that is,

$$W = \frac{dZ_c}{dt}, \quad (6a)$$

$$D_L = \frac{1}{2} \frac{d}{dt} \langle (Z - Z_c)^2 \rangle, \quad (6b)$$

$$D_T = \frac{1}{4} \frac{d}{dt} \langle R^2 \rangle. \quad (6c)$$

An example of this data is shown in Fig. 2. The max-

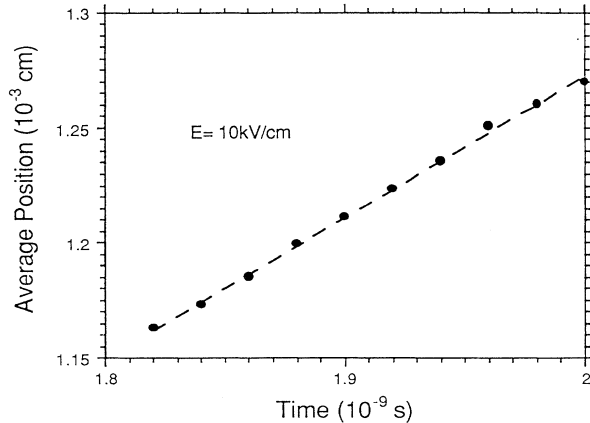


FIG. 2. Behavior of the center of mass of the electron assembly,  $z_c$ , versus time in the steady state regime.

imum percentage deviation of the data from the straight-line approximation is less than 0.5% for  $E = 10$  kV/cm. At the very high fields, the deviation in the  $\langle R^2 \rangle$  data can be as high as a few percent. The fluctuation in each quantity (i.e., variation from time section to section) has also been computed in the steady-state regime. The fluctuation in mean energy has been calculated to be less than 3% for all cases. The fluctuation in the macroscopic ionization rate is large since the largest field investigated is near its threshold value and consequently the number of particles being sampled is small.

### IV. SCATTERING RATES IN LIQUID ARGON

The implementation of the approach outlined in Sec. III requires knowledge of the total scattering rate,  $\Gamma_T(\epsilon)$ , the probabilities for the various types of scattering events, and the changes they cause on the state of the electron. The total scattering rate is given by

$$\Gamma_T(\epsilon) = \sum_i \Gamma_i(\epsilon) \quad (7)$$

with  $\Gamma_i(\epsilon)$  being the rate for event  $i$ . Consequently, the probability of event  $i$ ,  $P_i$ , is given by  $\Gamma_i/\Gamma_T$ .  $P_i$  determines the type of scattering event occurring at the end of the free flight.

The rates that have been used for the simulation of electron behavior in liquid argon are presented below. As mentioned in Sec. II, for the fields of interest in this paper (above 10 kV/cm), only the free-electron subassembly need be considered.

At energies above  $\epsilon_t$  (see Sec. III), where the free-electron states approach those of a dilute gas, the scattering potential is the complete microscopic potential. The interaction of these high-energy electrons with liquid argon result in two types of scattering: (a) diffuse (although the response of the liquid is neither a true collective mode nor that of an isolated atom, this type of scattering is reminiscent of phonon scattering in solids and "elastic" scattering with recoil in gases. It leads to the emission or absorption of a "quasiphonon"). And (b) electronic excitation of individual atoms (at threshold energies shifted from their isolated atom values. At the higher threshold energies, these are reminiscent of exciton states in solids; whereas, at the lower energies they correspond to those of the isolated atom).

The rate for diffuse scattering can be obtained using the concept of dynamic structure factor introduced by Van Hove.<sup>35,36</sup> The rate,  $d\Gamma_e$ , for emission of a "quasiphonon" of energy  $\hbar\omega$  resulting from a transition from a state of momentum  $\mathbf{p}_0$  to a final state with momentum  $\mathbf{p}$ , lying in a small solid angle  $d\Omega$  and in the energy interval  $\epsilon_0 + d\epsilon$  is

$$d\Gamma_e(\mathbf{p}, \mathbf{p}_0) = \frac{N}{4\pi} \left[ \frac{\epsilon_0 + \hbar\omega}{\epsilon_0} \right]^{1/2} S(q(\epsilon_0, \hbar\omega), \hbar\omega) \sigma_e(\epsilon_0, \theta) v d\hbar\omega, \quad (8)$$

where  $\hbar\omega$  is the energy of the quasiphonon,  $\sigma_e$  is the differential elastic scattering cross section for the isolated atom,  $v$  is given by Eq. (3),  $q$  is the magnitude of the

change in electron momentum [ $\mathbf{q} = \mathbf{p}_0 - \mathbf{p}$ , where  $\mathbf{p}_0$  and  $\mathbf{p}$  are related to the initial and final energies via Eq. (4)], and  $S(q, \hbar\omega)$  is the (coherent) dynamic structure factor. The rate for quasiphonon absorption,  $d\Gamma_a$ , can be found from detailed balance by substituting in Eq. (8)

$$S(-q, -\hbar\omega) = S(q, \hbar\omega) \exp(-\hbar\omega/kT).$$

The scattering rates for electronic excitation to the  $j$ th state,  $\Gamma_j$ , are also obtained from Eq. (8), with  $\sigma_e$  replaced by the corresponding isolated atom excitation rate.<sup>38</sup> The energy threshold values for excitation have been shifted from their values in the gas phase to reflect the effect of the surrounding molecules.<sup>29</sup> The ionization threshold in argon has been taken to be equal to  $\varepsilon_i - \Delta\varepsilon_i$ , where  $\Delta\varepsilon_i$  corresponds to the bottom of the conduction band in the liquid relative to its value in the gas phase<sup>29</sup> (see Fig. 1).

The sources for the elastic differential scattering cross section for argon,  $\sigma_e$ , are as follows: (i) for energies below 2 eV, Weyhreter *et al.*,<sup>39</sup> above 2 eV and angles below 100°, Srivastava *et al.*,<sup>40</sup> above 10 eV and angles between 100° and 155°, Vuscovic.<sup>41</sup> A phase shift expansion has been used to obtain the cross sections for all other angles and energies, with values normalized to obtain the total scattering cross sections of Ferch *et al.*<sup>42</sup> for energies up to 20 eV and extrapolated to 30 eV using the results of Jost *et al.*<sup>43</sup>

The dynamic structure factor has been obtained as follows. For momentum transfer in the range 1.0–4.4 Å<sup>-1</sup> and energy transfer in the range 0–10.6 meV, the experimental data of Sköld *et al.*<sup>44</sup> has been used. The theory of Vineyard<sup>45</sup> and Pathak and Singwi<sup>46</sup> has been used to extend the range of energy and momentum transfer such that integration over  $d\hbar\omega$  yields the structure factor,  $S(q)$ , of Eisenstein and Gingrich<sup>47</sup> for momentum transfer below 2.5 Å<sup>-1</sup>, and that obtained from the Percus-Yevick<sup>48</sup> equation with a hard sphere diameter of 3.4 Å for momentum transfers above 2.5 Å<sup>-1</sup>.<sup>49</sup>

The total emission  $\Gamma_e$  rate, for energies  $\varepsilon_0 > \varepsilon_i$ , is obtained by integrating Eq. (8) over all angles and quasiphonon energies. The total rates for the other processes (quasiphonon absorption and electronic excitation) are obtained in a similar fashion. The changes in electron energy and momentum due to the scattering are determined by the energy lost in the process and the angle into which the electron is scattered. Consequently, for diffuse scattering, the probability for the emission of a quasiphonon with energy  $\hbar\omega$  is given by

$$P_e = \int_0^{\hbar\omega} \int_0^{2\pi} d\Gamma_e / \Gamma_e. \quad (9)$$

While the probability for the scattering of an electron into an angle  $\theta$  due to quasiphonon emission is given by

$$P_\theta = \int_0^\theta \int_0^\infty d\Gamma_e / \Gamma_e. \quad (10)$$

The corresponding probabilities for quasiphonon absorption and electronic excitation are obtained from Eqs. (9) and (10) by substituting  $\Gamma_a$  and  $\Gamma_j$ , respectively, for  $\Gamma_e$ .

For energies below  $\varepsilon_i$ , since part of the microscopic potentials have been taken into account in the effective mass, the remaining perturbing potentials give rise to (a)

phononlike and (b) disorder scattering. In this work, the rate obtained by Ascarelli<sup>6</sup> has been used, scaled down by a factor of 4 in order to obtain continuity at the selected value for  $\varepsilon_i = 0.075$  eV. This value corresponds to the maximum energy for which the free path for disorder scattering is calculated. In order to have a smooth transition at this value of energy,  $\alpha$  has been taken to be 20 eV<sup>-1</sup>. For the fields of interest in this paper (above 10 kV/cm), this range of energy was found to play a minor role in determining the behavior of the assembly. Because of this, the rates given by Eq. (8) were subsequently used for the whole energy interval. Presently, the scattering rates in this energy range and in the transition region about  $\varepsilon_i$  are being reevaluated in order to obtain a smoother transition and be able to carry out calculations at lower fields.

The total effective cross section for quasiphonon emission (defined as  $\Gamma_e/Nv$ ) is shown in Fig. 3. Also shown for comparison is the total elastic scattering cross section in the dilute gas phase from Ferch *et al.*<sup>42</sup> and Jost *et al.*<sup>43</sup> Note that the Ramsauer minimum is still present in the liquid phase although slightly less pronounced and shifted toward lower energies. However, due to the limitations of Eq. (8) for evaluating the rates at the lower energies, this can only be taken as an indication of the actual behavior.<sup>28</sup> To elucidate the influence of the shape of the cross-section [ $\sigma_e$  in Eq. (8)], simulations have also been carried out with modified sets of cross sections, obtained from those presented (labeled set 1) as follows: (a) set 2, same as set 1 except that for energies below the minimum the effective cross section in the liquid phase is kept constant at its minimum value (i.e., no Ramsauer minimum); (b) set 3, in Eq. (8), the total gas phase cross section is used instead of the differential cross section,  $\sigma_e$ . For this set, the angular dependence of the scattering in the liquid phase is entirely due to the dynamic structure function; and (c) set 4, same as set 3 except that for energies below the minimum the effective cross section in the liquid phase is kept constant at its minimum value (i.e.,

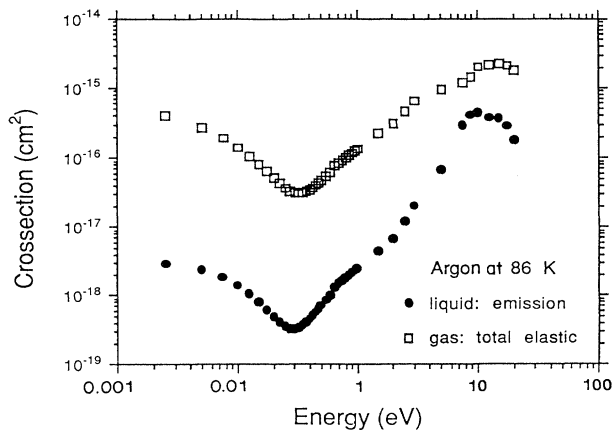


FIG. 3. Total liquid-phase quasiphonon emission rate,  $\Gamma_e$ , and total gas-phase elastic scattering rate vs energy for Argon at a temperature of 86 K and density of  $2.12 \times 10^{22} \text{ cm}^{-3}$ .

no Ramsauer minimum). Other variances have also been investigated [for example, using the gas-phase momentum transfer cross section in Eq. (8) instead of the differential cross section] but the results are similar to those obtained with the above sets. The results obtained with these four sets of cross sections are discussed in the next section.

Using Eqs. (1)–(10), a Monte Carlo algorithm can be developed to simulate the behavior of the electron assembly. Further details for developing such algorithm are given in Refs. 32 and 33.

## V. STEADY-STATE BEHAVIOR OF THE ELECTRON ASSEMBLY

### A. Energy distribution function

To elucidate the physics of the behavior of the electrons in liquid argon subjected to a constant electric field, the evolution to the steady state of an initial  $\delta$ -function distribution in energy has been simulated. The value taken for the initial electron energy has no effect on the steady-state results. The liquid temperature in the simulation is 86 K, since experimental data for drift velocity<sup>14–19</sup> and transverse diffusion coefficient<sup>20</sup> as a function of field are available.

The steady-state distribution for various applied fields is shown in Fig. 4. In the lower range of fields considered in this paper, as the field increases from its lowest value, electrons are heated up rapidly due to quasiphonon scattering and leading to a flattening of the distribution. The rapidly increasing scattering rate with electron energy “equilibrates” the tail of the distribution at an equivalent temperature,  $T_T$ , given from the average energy balance equation, by

$$kT_T = qEW / (\delta v_n), \quad (11)$$

where  $W$  is the drift velocity,  $\delta$  is an average energy loss

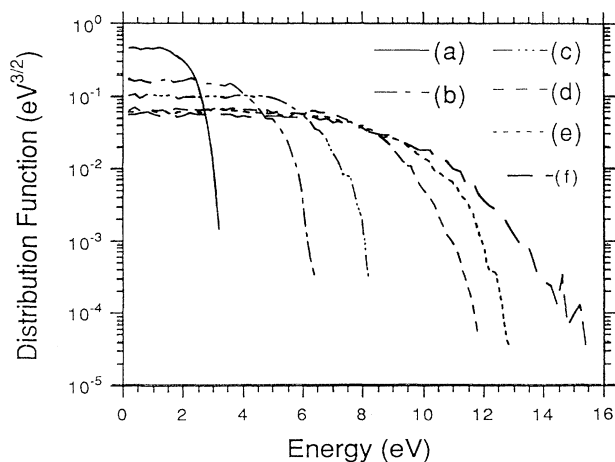


FIG. 4. Normalized electron energy distribution function in liquid argon,  $f(\epsilon)$ , vs energy, with applied field as a parameter. A straight line corresponds to a Maxwellian distribution. The fields in kV/cm corresponding to each of the curves are: (a) 10, (b) 90, (c) 200, (d) 500, (e) 1000, and (f) 2500.

factor, and  $v_n$  is a net (quasiphonon) emission rate. For  $E = 10$  kV/cm,  $v_n$ ,  $\delta$ , and  $W$  are found from the simulation to be  $1.6 \times 10^{12} \text{ sec}^{-1}$  (approximately)  $10^{-3}$ , and  $6.1 \times 10^5 \text{ cm/sec}$ , respectively. Equation (11) yields for  $kT_T \sim 3.8$  eV. A straight-line fit to the tail of the distribution [curve (a), Fig. 4] yields  $kT_T \sim 4.4$  eV, which is in reasonably good agreement. Note that Eq. (11) does not yield the mean energy (see Fig. 6 below) since the distribution is far from Maxwellian. Further increases in field (to tens of kV) causes the equilibration to occur at higher energies, but the tail temperature remains nearly constant (see Fig. 4). Similar behavior is observed in intervalley semiconductors as a result of the increase in intervalley scattering.<sup>33</sup> At a very large field (above 1 MV/cm), the equilibration occurs near the energy,  $\epsilon_m \sim 12$  eV which corresponds to the maximum in the total scattering rate. Consequently, the tail also begins to heat up and flatten. At fields above 3 MV/cm, some electrons in the tail are not equilibrated and become runaways.<sup>32</sup>

### B. Transport parameters and mean energy

The transport parameters and mean energy corresponding to the distributions shown in Fig. 4 are shown in Figs. 5–7. They have been calculated following the procedure described in Sec. III. The low-field range (near and below 10 kV/cm) corresponds to the small (positive) differential mobility regime (i.e., small  $dW/dE$ ), discussed in the literature.<sup>50</sup> The values obtained for the drift velocity up to 10 kV/cm are in good agreement with the experimental value<sup>15</sup> and those obtained by Sakai *et al.*, also using a Monte Carlo approach,<sup>51</sup> and Cohen and Lekner using a Boltzmann approach.<sup>1</sup> For increasing field, the faster than exponential increase in the total scattering rate, coupled to the increase in the backscattering rate with energy, gives rise to drift velocity saturation and to a regime with negative differential mobility. Although the negative differential mobility obtained in this work is smaller than that obtained by Sakai *et al.*<sup>51</sup> and Cohen and Lekner,<sup>1</sup> the overall behavior is very similar, and not in agreement with experiment. This behavior, as discussed below, is primarily due to the increase in the backscattering rate with energy, also noted by Sakai *et al.*<sup>51</sup> Since this behavior has not been observed experimentally and since no assumptions have been made in the Monte Carlo approach regarding the angular dependence of the distribution (such as the two-term spherical-harmonies expansion used by Cohen and Lekner<sup>1</sup>), simulations have been done with three other cross-section sets (see Sec. IV) to provide insight into the origin of the calculated negative differential mobility. The drift velocity, mean energy, and diffusion coefficients for fields of 200 kV/cm and 500 kV/cm (in the regime of negative differential mobility) and for each set of modified cross section is tabulated in Table I. Note that the behavior of the low-energy liquid phase cross sections has little effect on the results (largest effects are on the diffusion coefficients) in this range, as can be ascertained by comparing the results from set 1 [Eq. (8)], set 2 [Eq. (8) with cross sections below the minimum at 0.25 eV set equal to the minimum value], and set 4 [Eq. (8) with total gas

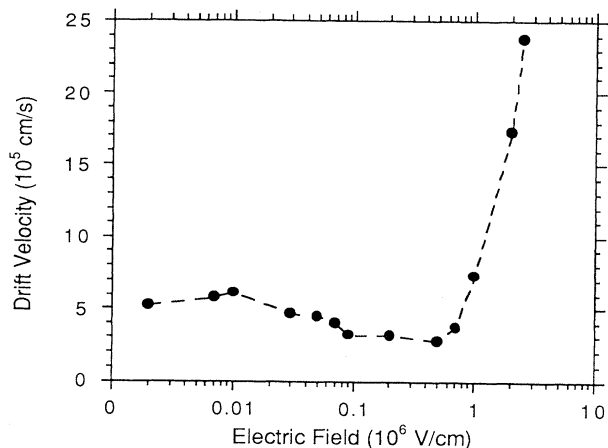


FIG. 5. Drift velocity  $W$  vs applied field. Note regime with negative differential mobility for fields in the range  $10 < E < 500$  kV/cm.

cross section and cross sections for energies below the minimum set equal to the minimum value]. Moreover, this observation also applies to the angular dependence of the gas phase scattering cross sections, as can be seen by comparing the results from set 1 [Eq. (8) with the gas phase differential scattering cross section] with those from set 4 (where the total gas phase cross section is used instead). These results are not surprising since the mean energy at these fields is well above the energy at the cross-section minimum. Thus, for a distribution function that is relatively flat as a function of energy (see Fig. 2), electrons with energies below the minimum have little effect on the average properties of the assembly. The results also show that the origin of the negative differential mobility lies with the increase in the backscattering rate with energy, which behavior stems from the dynamic structure function,  $S(\kappa, \omega)$ . It is not clear at present how to resolve this discrepancy with experiment. At sufficiently high fields, a significant number of electrons

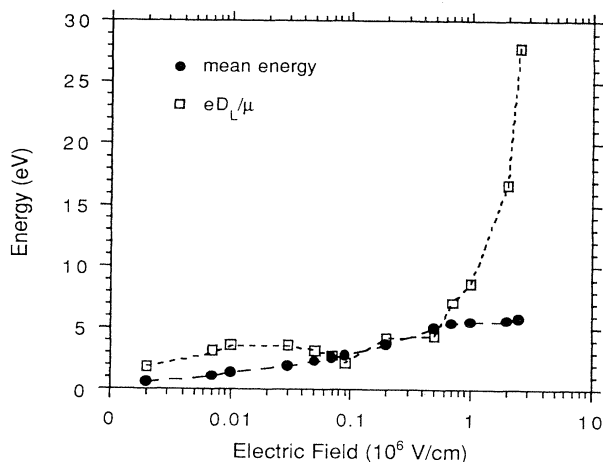


FIG. 6. Mean,  $\bar{\epsilon}$ , and characteristic,  $eD_L/\mu$ , energies vs applied field.

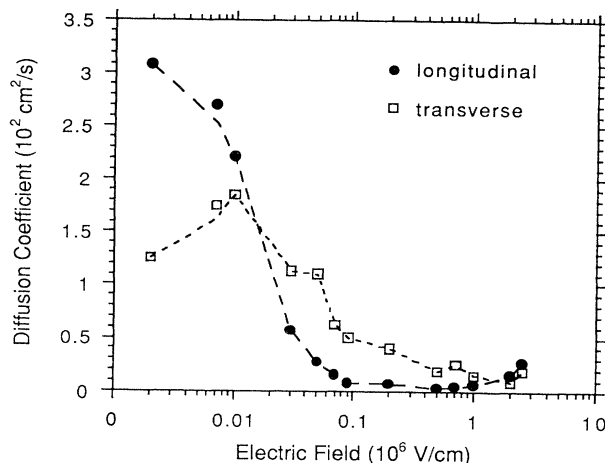


FIG. 7. Longitudinal  $D_L$  and transverse  $D_T$  diffusion coefficients vs applied field. Note the reversal in the magnitude between these coefficients at fields near 20 kV/cm and 1.5 MV/cm.

in the distribution are found at energies above the maximum in the backscattering rate (approximately 6 eV) and ultimately above  $\epsilon_m$ , so that the differential mobility again becomes positive and the drift velocity increases rapidly with field.

The mean-electron energy is shown in Fig. 6 to increase monotonically with field. For fields near  $10^5$  V/cm, the results for the mean energy presented are in reasonable agreement with those of Gushchin *et al.*,<sup>52</sup> however, at lower fields the discrepancy becomes significant (factor of 2 at 10 kV/cm). The characteristic energies,  $eD_L/\mu$  and  $eD_T/\mu$  have also been calculated from the results. For a Maxwellian distribution, these expressions are equal to the mean energy, and the differences in their values can be used as a measure of the departure from such a distribution. For all fields,  $eD_T/\mu$  has been found to be considerably higher than the mean energy. At 10 kV/cm,  $eD_T/\mu = 3$  eV, which is near the calculated temperature of the tail of the distribution (namely, 3.8 eV), but considerably higher than the mean energy of 1.4 eV. However, at higher fields, it also becomes considerably higher than the tail temperature (at 70 kV/cm,  $eD_T/\mu = 11$  eV, whereas the tail temperature is nearly constant in this range). Thus, it has not been possible to ascribe a physical significance to this energy. In contrast, the ratio  $eD_L/\mu$  has a smaller variation with field for fields below 500 kV/cm, and its value is closer to the tail temperature. This is in agreement with the observation that the tail of the distribution is Maxwellian in character as a result of equilibration in the presence of the field. At higher fields, it also follows the trend of the tail temperature. The behavior of this ratio with field is shown in Fig. 6.

The transverse and longitudinal diffusion coefficients are shown in Fig. 7. As the field increases, the ratio  $D_L/D_T$  is observed to become less than one for fields above 20 kV/cm, again becoming greater than one for

TABLE I. Comparison of results obtained with cross sections given by Eq. (8) (set 1) with those obtained with the modified cross-section sets (sets 2, 3, and 4, see text).

Cross-section set	$W$ ( $10^5$ cm/sec)	$D_L$ ( $\text{cm}^2/\text{sec}$ )	$D_T$ ( $\text{cm}^2/\text{sec}$ )	$\bar{\epsilon}$ (eV)	
1	3.1	5.5	39.7	3.6	$E = 200$ kV/cm
2	3.4	2.5	47.5	3.65	
3	3.3	3.7	40.0	3.64	
4	3.1	4.25	45.0	3.7	
1	2.7	2.7	18.6	5.0	$E = 500$ kV/cm
2	2.5	2.45	24.7	4.8	
3	2.6	1.4	25.0	5.0	
4	2.7	1.7	27.5	4.9	

fields above 1 MV/cm. Both reversals arise from a combination of having high (low) energy electrons at the front (back) of the assembly (see Fig. 8, where the radially integrated mean energy is shown as a function of axial position; the fluctuation in energy at the front of the assembly

are due to the small number of electrons being sampled) and the energy and angle dependence of the scattering rate.

At the front, the increase in energy of the electrons brought about by the electric field acting on the longitudinal diffusion current<sup>53,54</sup> leads to a decrease in the local drift velocity with increasing field above 10 kV/cm. At these fields, a large fraction of the electrons are going through the minimum in the scattering rate with energy. For increasing fields above 1 MV/cm, the energy increase leads to an increase in the local drift velocity since the forward scattering increases with energy (i.e., the distribution becomes more anisotropic toward the front). At the rear of the assembly, the diffusion current acting against the field leads to a decrease in energy and a concomitant change in the local drift velocity. This velocity increases with field above 10 kV/cm, whereas it decreases with increasing field above 1 MV/cm.

As a consequence of the behavior of the local drift velocity at the front and rear, the assembly contracts longitudinally (relative to its radial behavior) with increasing field above 10 kV/cm resulting in a relative decrease in  $D_L$  with respect to  $D_T$  and thus a decrease in their ratio. With increasing field above 1 MV/cm, the assembly expands longitudinally resulting in an increase in the  $D_L/D_T$  ratio. The behavior of  $D_L/D_T$  with field may be used as an additional experimental test for the characteristics of the Ramsauer minimum in liquid argon. There are no measurements of the diffusion coefficients at these values of field with which to compare the results presented.

### C. Ionization rate

Macroscopic (moment) descriptions of electron dynamics require knowledge of the rate coefficients that appear in the corresponding equations. In a one-moment description (in terms of the continuity equation for electron density), the necessary rates are the averaged free electron gain or loss rates. For the applied fields considered in this paper, the effective loss rate (due to trapping/detrapping) is essentially zero. The focus in this regime is on the dependence of the ionization rate on the applied field. This issue is most important for determining the breakdown mechanism in the liquid phase.

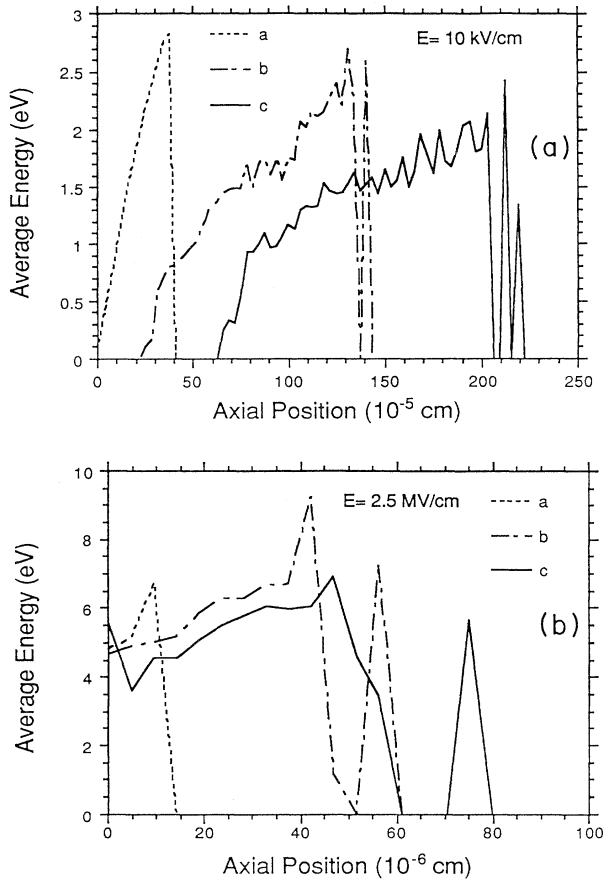


FIG. 8. Radially integrated, mean electron energy vs axial positions with times as parameter for applied fields of 10 kV/cm and 2.5 MV/cm. The times,  $t$ , corresponding to each of the curves are (a): (a) 0.08 ns, (b) 1.04 ns, and (c) 2.0 ns; in (b): (a) 0.6 ps, (b) 7.8 ps, and (c) 15.0 ps.

TABLE II. Ionization rate in liquid argon.

Applied field (MV/cm)	Ionization rate (sec <sup>-1</sup> )
1	2.8 × 10 <sup>5</sup>
2	1.0 × 10 <sup>9</sup>
2.5	3.4 × 10 <sup>9</sup>

The ionization rate has been computed from the relation

$$Nv_i = \int \Gamma_i(\epsilon) f(\epsilon) \epsilon^{1/2} d\epsilon, \quad (12)$$

where  $\Gamma_i$  is the energy dependent ionization rate obtained from Eq. (8) with  $\sigma_e$  replaced by  $\sigma_i$ , the ionization cross section;  $N$  is the liquid density; and the threshold energy for ionization (i.e., the band gap) is taken to be equal to 15.6 eV. The results are shown in Table I.

The threshold field for ionization is found to be slightly below 2 MV/cm. There are no experimental values available for ionization rate in liquid argon. Electron avalanches have been observed in liquid xenon at lower fields,<sup>55</sup> as would be expected, since the ionization threshold is lower.

## VI. CONCLUDING REMARKS

A model for the motion of an electron in a simple liquid has been presented in Sec. II. This model has been used to implement a Monte Carlo simulation of the behavior of an electron assembly in liquid argon. To accomplish this, a set of scattering rates for electrons in liquid argon have been obtained and presented in Sec. IV. The steady-state behavior of the assembly in the presence of a dc electric field has been investigated. The dependence of the energy distribution, transport parameters, and ionization rate on electric field has been obtained. At the lower values of field, the calculated value of drift velocity is in good agreement with experiments and previ-

ous calculations. As the field increases above 10 kV/cm, a region of negative differential mobility has been observed. This behavior, although in qualitative agreement with previous calculations, is not in agreement with experiments. A positive differential mobility is again observed for fields above 100 kV/cm when a substantial number of the electron population is in the energy range above the peak in the backscattering rate. For fields above 3 MV/cm, a significant number of electrons in the distribution are found with energies above that corresponding to the maximum in the total scattering rate. A small percentage of these electrons can gain more energy from the field than they transfer to the liquid and thus become runaways. This is reflected in the field dependence of the ratio  $D_L/D_T$  which has been found to become greater than one above 1.5 MV/cm.

In order to determine the mechanism leading to the electric breakdown of liquids, it is important to assess the dependence of the ionization rate with electric field. It has been shown that for fields above 2 MV/cm, the energy distribution extends beyond the threshold for electron impact ionization, yielding a nonzero value for the ionization rate. Thus, above this field, electron avalanches can develop. Such avalanches have been observed in liquid xenon (at lower values of field since the ionization threshold is lower). Presently, there are no experimental results at the higher fields for the longitudinal and transverse diffusion coefficients with which to compare the results presented.

As pointed out in the paper, a number of discrepancies remain to be resolved. To do so will require further improvements in the values presented for the scattering rates and the dispersion equation, Eq (4a), particularly near the transition region between the gaslike and solidlike representations.

## ACKNOWLEDGMENTS

I would like to thank J. Bentson for his invaluable assistance with the computations. This work is supported by the U.S. Office of Naval Research.

<sup>1</sup>M. H. Cohen and J. Lekner, Phys. Rev. **158**, 305 (1967).

<sup>2</sup>G. L. Braglia and V. Dellacasa, Phys. Rev. A **18**, 711 (1978).

<sup>3</sup>T. F. O'Malley, Phys. Rev. **130**, 1020 (1963); J. Phys. B **13**, 1491 (1980).

<sup>4</sup>M. Atrazhev, J. Phys. D **17**, 889 (1984).

<sup>5</sup>S. Basak and M. H. Cohen, Phys. Rev. B **20**, 3404 (1979).

<sup>6</sup>G. Ascarelli, Phys. Rev. B **33**, 5815 (1986); **34**, 4278 (1986).

<sup>7</sup>A. I. Gubanov, *Quantum Electron Theory of Amorphous Conductors* (Consultants Bureau, New York, 1965).

<sup>8</sup>N. R. Kestner and J. Jortner, J. Chem. Phys. **59**, 16 (1973).

<sup>9</sup>B. I. Shkolovskii and A. L. Efros, *Electronic Properties of Doped Semiconductors* (Springer-Verlag, New York, 1984).

<sup>10</sup>H. T. Davis, L. D. Schmidt, and R. M. Minday, Chem. Phys. Lett. **13**, 413 (1972).

<sup>11</sup>R. Schiller, S. Vass, and J. Mandics, Int. J. Rad. Phys. Chem. **5**, 491 (1973).

<sup>12</sup>J. P. Dodelet, K. Shinsaka, and G. R. Freeman, Can. J. Chem. **54**, 744 (1976).

<sup>13</sup>J. K. Baird and R. H. Rehfeld, J. Chem. Phys. **86**, 4090 (1987).

<sup>14</sup>S. S. Huang and G. R. Freeman, Phys. Rev. A **24**, 714 (1981).

<sup>15</sup>L. S. Miller, S. Howe, and W. E. Spear, Phys. Rev. **166**, 871 (1968).

<sup>16</sup>G. Bakale, W. Tauchert, and W. F. Schmidt, J. Chem. Phys. **63**, 4470 (1975).

<sup>17</sup>I. Gyorgy and G. R. Freeman, J. Electrostatics **7**, 239 (1979).

<sup>18</sup>N. E. Cipollini and R. A. Holroyd, J. Chem. Phys. **67**, 4636 (1977).

<sup>19</sup>R. A. Holroyd, K. Itoh, K. Nakagawa, M. Nishikawa, and K. Fueki, J. Phys. Chem. **91**, 4639 (1987).

<sup>20</sup>E. Shibusura, T. Takahashi, S. Kubota, and T. Doke, Phys. Rev. A **20**, 2547 (1979).

<sup>21</sup>G. R. Freeman, *Kinetics of Nonhomogeneous Processes* (Wiley, New York, 1987), Chap. 2.

<sup>22</sup>W. F. Schmidt, Can. J. Phys. **55**, 2197 (1977).

<sup>23</sup>V. M. Atrazhev and I. T. Yakubov, Appl. Vys. Temp. **18**, 1292 (1980).

- <sup>24</sup>L. I. Schiff, *Quantum Mechanics* (McGraw Hill, New York, 1955).
- <sup>25</sup>J. M. Ziman, *Theory of Solids* (Cambridge University Press, Cambridge, England, 1979).
- <sup>26</sup>V. V. Atonin, Y. M. Galperin, V. L. Gurevich, and A. Schmid, *Phys. Rev. A* **36**, 5729 (1987).
- <sup>27</sup>F. Seitz, *The Modern Theory of Solids* (McGraw-Hill, New York, 1940).
- <sup>28</sup>L. Christophorou, in *The Liquid State and Its Electrical Properties*, Vol. 193 of NATO Advanced Study Institute, Series B: Physics, edited by E. E. Kunhardt, L. G. Christophorou, and L. H. Luessen (Plenum, New York, 1988), p. 283.
- <sup>29</sup>I. T. Steinberger, in *The Liquid State and Its Electrical Properties* (Ref. 28), p. 235.
- <sup>30</sup>N. F. Mott and E. A. Davis, *Electronic Processes in Non-Crystalline Materials* (Clarendon Press, Oxford, 1971).
- <sup>31</sup>C. Jacoboni and L. Reggiani, *Rev. Mod. Phys.* **55**, 645 (1983).
- <sup>32</sup>E. E. Kunhardt and Y. Tzeng, *J. Comput. Phys.* **67**, 279 (1985).
- <sup>33</sup>M. Cheng and E. E. Kunhardt, *J. Appl. Phys.* **63**, 2322 (1988).
- <sup>34</sup>E. Cohen and W. Thirring, editors, *The Boltzmann Equation*, *Acta Phys. Austriaca Sup. X* (Springer, Berlin, 1973).
- <sup>35</sup>L. Van Hove, *Phys. Rev.* **95**, 249 (1954).
- <sup>36</sup>N. H. March and M. P. Tosi, *Atomic Dynamics in Liquids* (Wiley, New York, 1976).
- <sup>37</sup>J. A. Jahnke, N. A. W. Holzwarth, and S. A. Rice, *Phys. Rev. A* **5**, 463 (1972).
- <sup>38</sup>L. Klein (private communication).
- <sup>39</sup>M. Weyhreter, B. Barzick, A. Mann, and F. Linder, *Z. Phys. D* **7**, 333 (1988).
- <sup>40</sup>S. K. Srivastava, H. Tanaka, A. Chutjian, and S. Trajmar, *Phys. Rev. A* **23**, 2156 (1981).
- <sup>41</sup>L. Vuscovic (private communication).
- <sup>42</sup>J. Ferch, B. Granitza, C. Masche, and W. Raith, *J. Phys. B* **18**, 967 (1985).
- <sup>43</sup>K. Jost, P. G. F. Bisling, F. Eschen, M. Felsmann, and L. Walther, in *Proceedings of the 13th International Conference on Physics of Electronic and Atomic Collisions*, edited by J. Eichler (North-Holland, Amsterdam, 1983), p. 91.
- <sup>44</sup>K. Sköld, J. M. Rowe, G. Ostrowski, and P. D. Randolph, *Phys. Rev. A* **6**, 1107 (1972).
- <sup>45</sup>G. H. Vineyard, *Phys. Rev.* **110**, 999 (1958).
- <sup>46</sup>K. N. Pathak and K. S. Singwi, *Phys. Rev.* **2**, 2427 (1970).
- <sup>47</sup>A. Eisenstein and N. S. Gringrich, *Phys. Rev.* **62**, 261 (1942).
- <sup>48</sup>J. K. Percus and G. J. Yevick, *Phys. Rev.* **110**, 1 (1958).
- <sup>49</sup>N. W. Ascroft, *Physica* **35**, 148 (1967).
- <sup>50</sup>W. F. Schmitt, in *The Liquid State and Its Electrical Properties* (Ref. 28), p. 273.
- <sup>51</sup>Y. Sakai, K. Sukegawa, S. Nakamura, and H. Tagashira, *IEEE Trans. Elec. Ins.* **23**, 609 (1988).
- <sup>52</sup>E. M. Gushchin, A. A. Kruglov, and I. M. Obodorskii, *Zh. Eksp. Teor. Fiz.* **82**, 1114 (1982) [*Sov. Phys. JETP* **55**, 650 (1982)].
- <sup>53</sup>J. H. Parker, Jr. and J. J. Lowke, *Phys. Rev.* **181**, 290 (1969).
- <sup>54</sup>L. G. Huxley and R. W. Crompton, *The Diffusion and Drift of Electrons in Gases* (Wiley, New York, 1974).
- <sup>55</sup>S. E. Derenzo, T. S. Mast, H. Zaklad, and R. A. Muller, *Phys. Rev. A* **9**, 2582 (1974).